Depletion of *ALMS1* inhibits TGF-β/SMAD3/SNAI1 axis altering normal cell migration capacity and epithelial-mesenchyme transition.

Brais Bea-Mascato[1,2], Elena Neira-Goyanes[1,2], Antía Iglesias-Rodríguez[1,2], Diana Valverde[1,2*]

1 CINBIO, Universidad de Vigo, 36310, Spain.

2 Grupo de Investigación en Enfermedades Raras y Medicina Pediátrica, Instituto de Investigación Sanitaria Galicia Sur (IIS Galicia Sur), SERGAS-UVIGO, Vigo, Spain

*Correspondence: Diana Valverde

CINBIO Facultad de Biología, Universidad de Vigo, Campus As Lagoas-Marcosende s/n, 36310 Vigo, Spain

Tel +34 986 811 953

Email dianaval@uvigo.es

ABSTRACT:

Background:

ALMS1 is a ubiquitous gene associated with Alström syndrome (ALMS). The main symptoms of ALMS affect multiple organs and tissues, generating at last, multi-organic fibrosis in the lungs, kidneys and liver. TGF-β is one of the main pathways implicated in fibrosis, controlling the cell cycle, apoptosis, cell migration, and epithelial-mesenchymal transition (EMT). Nevertheless, the role of *ALMS1* gene in fibrosis generation and other implicated processes such as cell migration or epithelial-mesenchymal transition via the TGF- β pathway has not been elucidated yet.

Methods:

Initially, we evaluated how depletion of *ALMS1* affects different processes like apoptosis, cell cycle and mitochondrial activity. Then, we performed proteomic profiling with TGF-β stimuli in HeLa ALMS1 -/- cells and validated the results by examining different EMT biomarkers using qPCR. The expression of these EMT biomarkers was validated in hTERT-BJ-5ta. Finally, we also evaluated the SMAD3 phosphorylation in BJ-5ta model and its cell migration capacity.

Results:

Depletion of *ALMS1* generated apoptosis resistance to thapsigargin (THAP) and C2-Ceramide (C2-C), and G2/M cell cycle arrest in HeLa cells. For mitochondrial activity, results did not show significant differences between *ALMS1 +/+* and *ALMS1 -/-*. Proteomic results showed inhibition of downstream pathways regulated by TGF-β. The protein-coding genes (PCG) were associated with processes like focal adhesion or cell-substrate adherens junction. EMT biomarkers *VIM*, *DSP*, and *SNAI1* showed an opposite pattern to what would be expected when activating the EMT. Finally, inhibition of *SNAI1* was consistent in BJ-5ta model, where a reduced activation of SMAD3 and a decrease in migratory capacity were also observed.

Conclusion:

ALMS1 has a role in controlling the cell cycle and the apoptosis processes. Moreover, the depletion of *ALMS1* inhibits the signal transduction through the TGF-β/SMAD3/SNAI1, which could be affecting the cell migration capacity and EMT.

Keywords: ALMS1, Alström syndrome, ciliopathies, primary cilia, TGF-β, epithelial-mesenchymal transition (EMT), fibrosis, cell cycle arrest, apoptosis.

INTRODUCTION:

ALMS1 is a ubiquitous gene with 23 exons located on chromosome 2p13. Mutations in this gene are related to Alström syndrome (ALMS; OMIM #203800), a rare, autosomal and recessive disease with a prevalence of 1-9 cases per 1.000.000 inhabitants and approximately 950 cases reported worldwide (Orphanet). The main symptoms of ALMS affect multiple organs and tissues [1], such as cone-rod retinal dystrophy, dilated cardiomyopathy (DCM) and hypertension [2], hypertriglyceridemia, type II diabetes mellitus (T2D) [3], and hepatic, renal and pulmonary dysfunction caused by multi-organic fibrosis [1], [4], which is the main cause of death in these patients.

The protein encoded by *ALMS1* plays a structural role in the eukaryotic cell centrosomes [5], a microtubule (MT)-nucleating organelle strongly related to primary cilia. The ALMS1 basal body location [5], [6] has been related to different functions controlled by the primary cilium such as centrosome cohesion, cell cycle control and endosomal trafficking [6]–[9].

Although numerous roles of ALMS1 have been described at both ciliary and extraciliary levels, the regulation of the pathways underlying these cellular processes remain unknown. Recently, our group has established the relationship between the *ALMS1* gene and the TGF-β signaling pathway [10], which could be related to the development of fibrosis in these patients [11], [12]. TGF-β is a signalling pathway regulated by clathrin-dependent endocytosis (CDE) in the pocket region of primary cilium [13], and coordinates cell cycle, apoptosis and migration processes such as epithelium-mesenchyme transition (EMT) [14]. This pathway acts in close coordination with other signalling cascades such as Wnt, Hippo, Notch, Hedgehog (Hh), mitogen-activated protein kinase (MAPK), and phosphoinositide 3-kinase (PI3K)-Akt, resulting in many cases in complex regulatory networks dependent on the primary cilium [15].

Stimulation of the TGF-β pathway can activate two main cascades: the canonical (SMAD-dependent) pathway and the non-canonical (SMAD-independent) pathway [16]. The canonical pathway is coordinated by transcription factors called R-SMAD (SMAD2 and SMAD3) which join co-SMAD (SMAD4) to activate the expression of several genes such as *SNAI1* [17], [18], a key modulator of EMT [19], [20]. This pathway is inhibited by an I-SMAD, SMAD7, which inhibits R-SMAD signalling in a variety of ways, binding to TGF-β receptors or directly in the nucleus, avoiding the binding of the R-Smad-Smad4 complex to DNA [21]. On the other hand, the non-canonical activation pathway includes a wide group of pathways such as p38 MAPK, PI3K/AKT, or Rho GTPases [16].

In this context, the role of *ALMS1* in the regulation of the TFG-β pathway remains unknown. Understanding how the absence of *ALMS1* controls cell migration processes such as EMT through the TGF-β pathway is key to understanding how the multi-organ fibrosis occurs in these patients.

In this article, we studied how the lack of *ALMS1* affects different cell processes such as mitochondrial activity, cell cycle, apoptosis, and signal transduction through the TGF-β pathway. Moreover, we evaluated the expression pattern for different EMT biomarkers after TGF-β pathway stimulation in two independent CRISPR-KO cell models (HeLa and BJ-5TA) for *ALMS1*. Finally, we measured p-SMAD3 activation and migration capacity in the BJ-5ta line in the presence of the TGF-β1 ligand.

RESULTS:

ALMS1 depletion does not alter mitochondrial basal activity despite generating G2/M cell cycle arrest in HeLa cells:

ALMS1 is a structural centromere protein [5] that controls the structure of the cytoskeleton [22]. Since *ALMS1* depletion causes cell cycle elongation [8], [23] it is expected that mitochondrial activity will also be altered, as both processes are dependent on each other and regulated by cytoskeletal dynamics. [24].

We evaluated the different phases of the cell cycle using the fox synchronous algorithm [25] to determine the Gaussian distribution of the different populations. In the plots, an initial population was defined to isolate cells from debris. Next, DAPI fluorescence (461 nm) and events count (cells) were displayed in the plots, and the algorithm was applied to plots (Figure 1.A). After 24h of incubation, we determined that *ALMS1* -/- genotype in HeLa cells significantly reduced (p-value < 0.05) the percentage of the cell population in S phase from 24.26 % ± 1.32 in *ALMS1* +/+ to 19.27 % ± 1.69 in *ALMS1* -/-. The cell cycle arrest was caused by a significant increase in the G2/M population (p-value < 0.01), from 1.6% ± 0.62 in *ALMS1* +/+ to 4.88 % ± 0.80 (Figure 1.B). The results in the G0/G1 population did not show significant differences between genotypes. Despite this, the basal mitochondrial activity did not show a significant difference between *ALMS1* +/+ and *ALMS1* -/- (Figure 1.C).

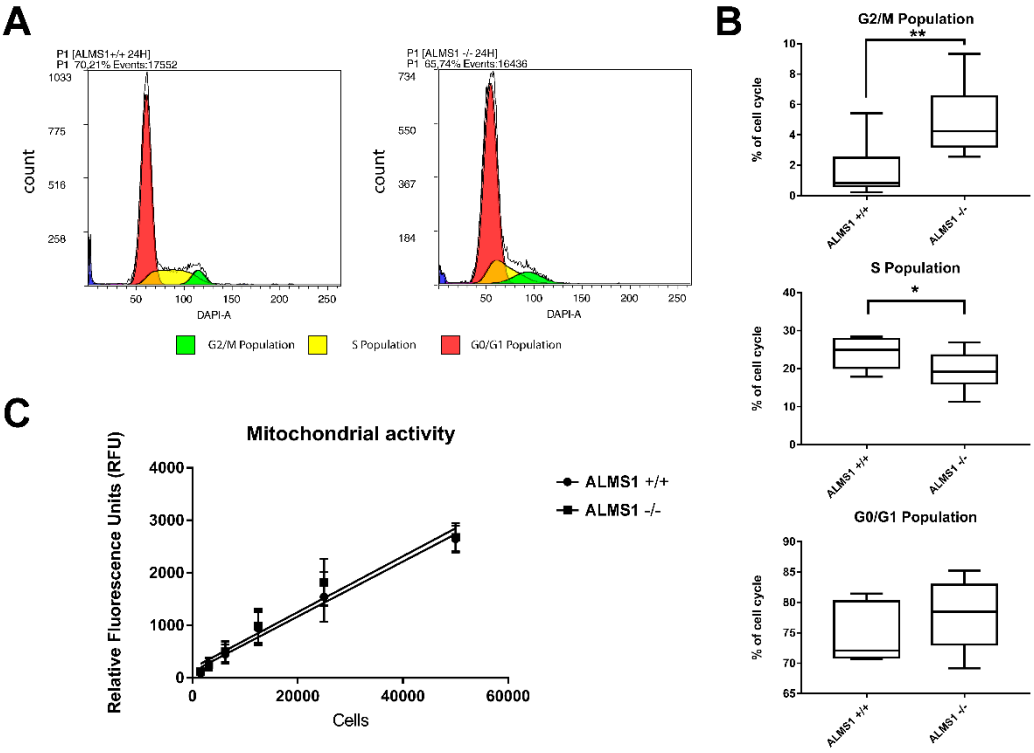

Figure 1. Cell cycle assay and mitochondrial activity results. **(A)** Cytometry plots with DAPI fluorescence and events count. Colours correspond with each population defined by fox synchronous algorithm. **(B)** Box-plot for each population previously defined in the cytometry plot that represents the percentage of cell cycle populations from parent population. **(C)** Linear regression between relative fluorescence units (RFU) and cell concentration in both genotypes (*ALMS1 +/+* and *ALMS1 -/-*). This experiment was carried out in triplicate and repeated 3 times on different days (N=3, n=3). *: p-value < 0.05, **: p-value < 0.01.

The lack of *ALMS1* in HeLa prevents apoptosis induced by C2-ceramides and Thapsigargin:

Accumulation of cells in G2/M phase triggers apoptosis by different pathways such as caspases [26], [27]. We evaluated whether these cells were sensitive to apoptosis in response to an ER stress-inducing stimulus (Thapsigargin; THAP) [28], and a pro-apoptotic sphingolipid such as C2-ceramide.

As in the cell cycle assay, initial isolation of the cell population of interest was performed and named as P1. In the P1 population, plots were represented with the FL4 (7-AAD) fluorescence in the y-axis and FL1 (Annexin V) fluorescence in the x-axis, both on a logarithmic scale. Thresholds for different populations (viable, early apoptotic, late apoptotic, and necrotic) were defined by a previous compensation analysis using THAP-like positive control of cell death. Finally, experiments were performed by triplicates in the plate (n=3) and in 3 alternative days (N=3).

The results showed a significant difference between the genotypes *ALMS1* +/+ and *ALMS1* -/- in viable (44.02% and 69.49%, respectively) and early apoptotic (43,47% and 23,44%) populations in cells stimulated with C2-C (Figure 2.A-B), and viable (49,56% and 71,33%), early apoptotic (18,25% and 8,56%) and late apoptotic (25,09% and 11,93%) populations in cells stimulated with THAP (Figure 2.C-D). These results indicate a resistance to apoptosis for these stimuli due to the lack of the *ALMS1*.

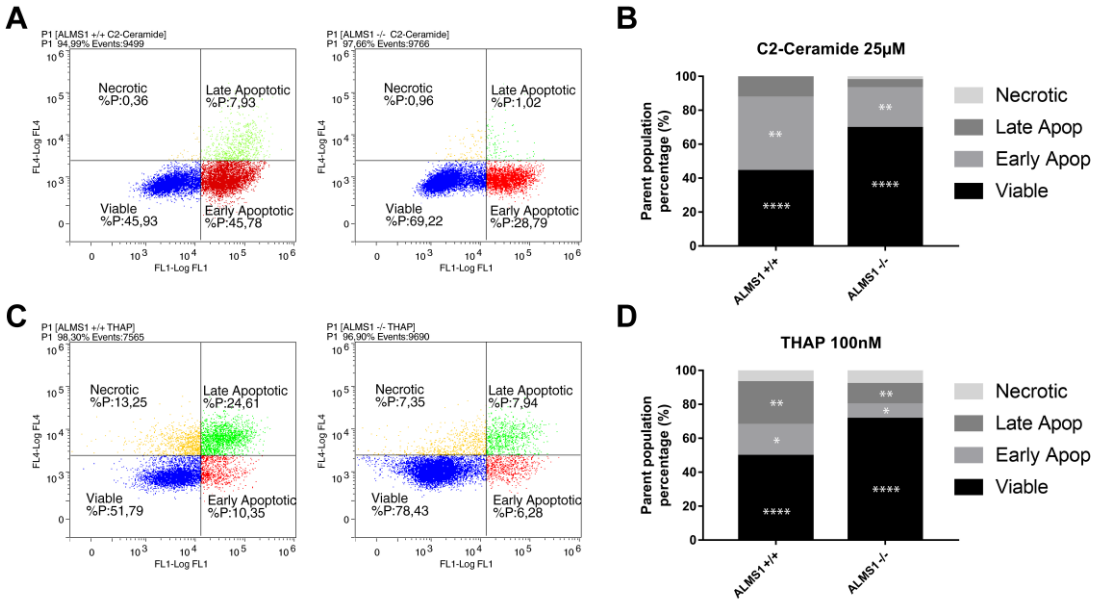

Figure 2. Apoptosis assay by annexin-V IP. **(A)** Cytometry plots for C2-ceramide (C2-C) with Log FL4 channel (IP) vs Log FL1 channel (Annexin-v). **(B)** Stacked-bar graph for cells treated with C2-C in a concentration of 25 µM. Percentages of each population are represented from a parent population previously defined. **(C)** Cytometry plots for thapsigargin (THAP) with Log FL4 channel (IP) vs Log FL1 channel (Annexin-v). **(D)** Stacked-bar graph for cells treated with THAP in a concentration of 100 nM. Percentages of each population are represented from a parent population previously defined. This experiment was carried out in triplicate and repeated 3 times on different days (N=3, n=3). *: adj. p-value < 0.05, **: adj. p-value < 0.01, ***: adj. p-value < 0.001, ****: adj. p-value < 0.0001.

The proteomic profile in HeLa cells reveals *ALMS1* like a regulator of Epithelium Mesenchymal Transition through the TGF-β pathway:

TGF-β is a pathway that plays a key role in the control of cell proliferation and apoptotic processes [14]. Since signal transduction through this pathway occurs via the primary cilium [13], [29], the lack of *ALMS1* could explain the aberrant processes seen above.

We evaluated how *ALMS1* depletion affects the signal transduction through TGF-β pathway. In this bulk analysis, we obtained a total of 86 differentially expressed proteins (DEP) (Figure 3.A), 31 (36%) over-expressed and 55 (64%) under-expressed. From this dataset, a total of 76 proteins were associated with genes (Figure 3.C).

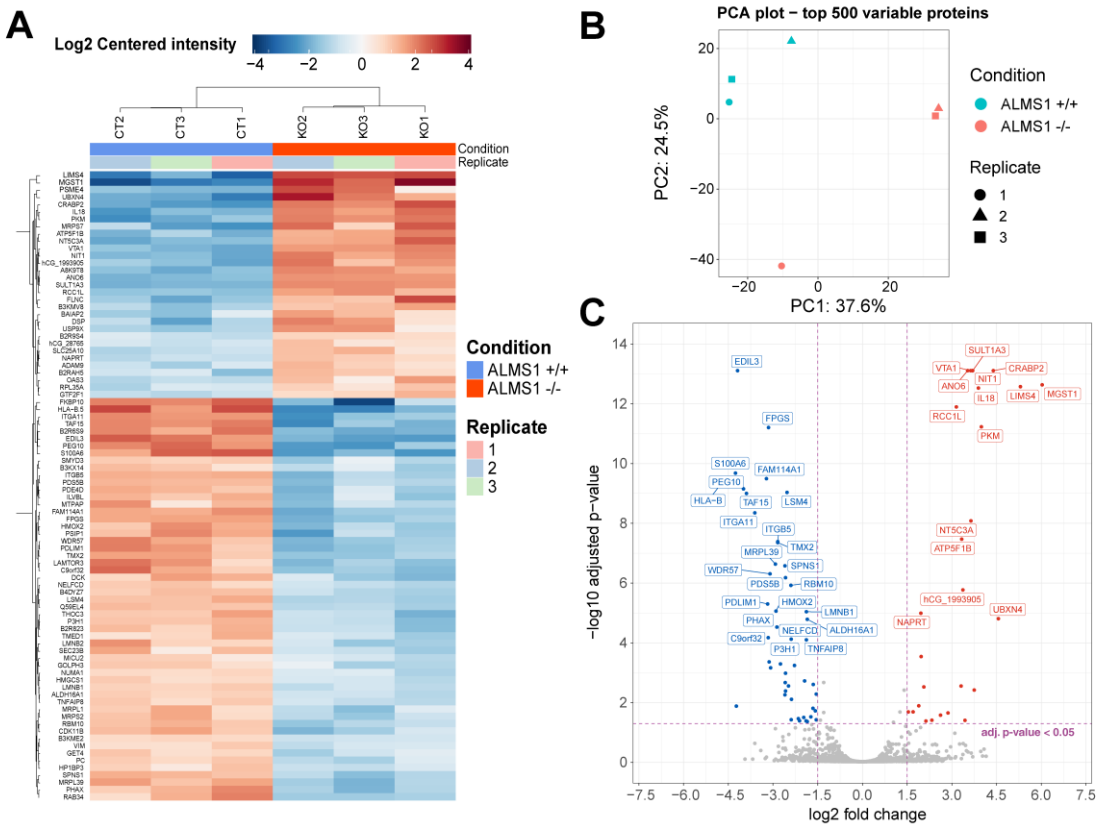

Figure 3. Differential expression analysis for proteomic data in HeLa. **(A)** Heatmap for all proteins (associated and not associated with genes) differentially expressed. Plot shows the expression pattern for the 3 biological replicates of genotype *ALMS1 +/+* (CT) and genotype *ALMS1 -/-* (KO). **(B)** Principal components analysis (PCA) for the top 500 variable proteins with all biological replicates for each genotype. **(C)** Volcano-plot showing the top 40 most significant genes associated with proteins. Proteins with no clear gene association were removed from this plot. Significant thresholds: log2 FC > 1.5, adj. p-value < 0.05. This experiment was carried out in triplicate (n=3).

Based on the DE of protein-coding genes (PCG) we performed an enrichment analysis obtaining a total of 9 GO terms significantly overrepresented (adj. p-value < 0.05) (Figure 4. A-B). The majority of these PCG were associated with focal adhesion, cell-cell or cell-matrix interactions. This result suggests the implication of *ALMS1* in the control of adhesion processes through the TGF-β pathway. In addition, we calculated the z-score of these GO terms (Figure 4.A), which showed a significant decrease in the ability of these cells to properly migrate or adhere to each other or their matrix.

Finally, genes such as vimentin (*VIM*) and desmoplakin (*DSP*), common biomarkers of EMT, were associated with these GO terms (Figure 4.B). Interestingly, these genes exhibited an expression pattern opposite to that observed for the EMT process.

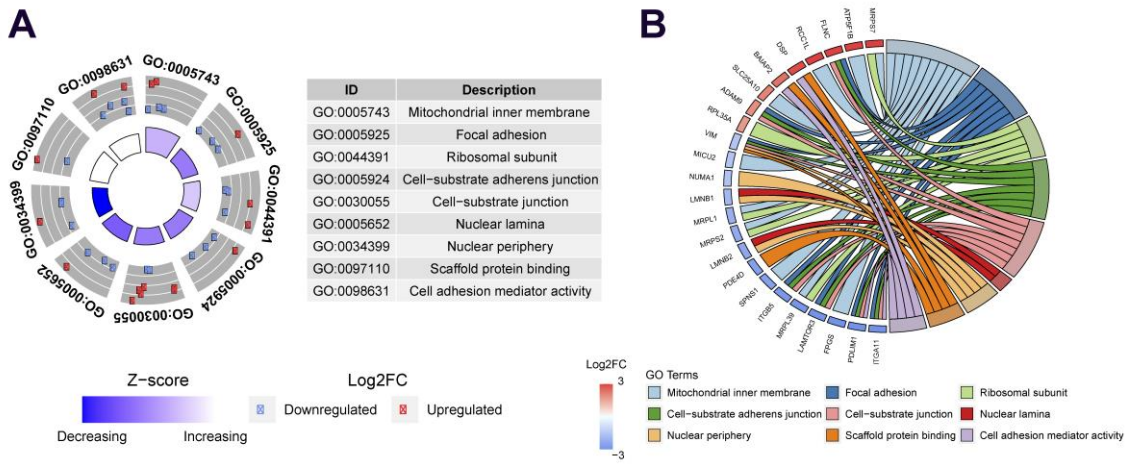

Figure 4. Enrichment analysis based on Go terms for proteomic data. **(A)** GoCircle-plot that includes significant over-represented GoTerms in a table (ID and Name) and scatter plot with FC of any gene related with each GoTerm. Moreover, this plot includes Z-score which is an estimation of up-regulation or down-regulation in the Goterm. **(B)** Circus-Plot applied to Goterms to relate any Gene name with the corresponding GoTerm name. The plot also shows the FC of each gene and the list is sorted by FC from the most over-expressed (3) up to the most under-expressed (-3).

ALMS1 depletion alters the expression pattern of TGF-β1-induced EMT markers in HeLa:

VIM is a key player in the regulation of EMT and its deficiency leads to inhibition of this process [30]. On the other hand, *DSP* is a protein involved in cell-cell junctions mediated by desmosomes. It is therefore considered a typical epithelial marker whose decrease is related to the passage of the cell from an epithelial to a mesenchymal state [31].

The overexpression of DSP, together with the underexpression of VIM upon stimulation of the TFG-β pathway, seems to be two clear signals that EMT might be inhibited when *ALMS1* is removed. We evaluated the expression of the principal EMT biomarkers (*SNAI1*, *CDH2*, *TWIST1*, *ACTA2*, *VIM,* and *DSP*) and other genes related to EMT (*POSTN*, *EDIL3*). We perform stimulations at different times (24, 48 and 72 hours) with rh-TGF-β1 (2ng/µL), obtaining the same expression pattern in the 3 experiments performed (Figure 5.A-C).

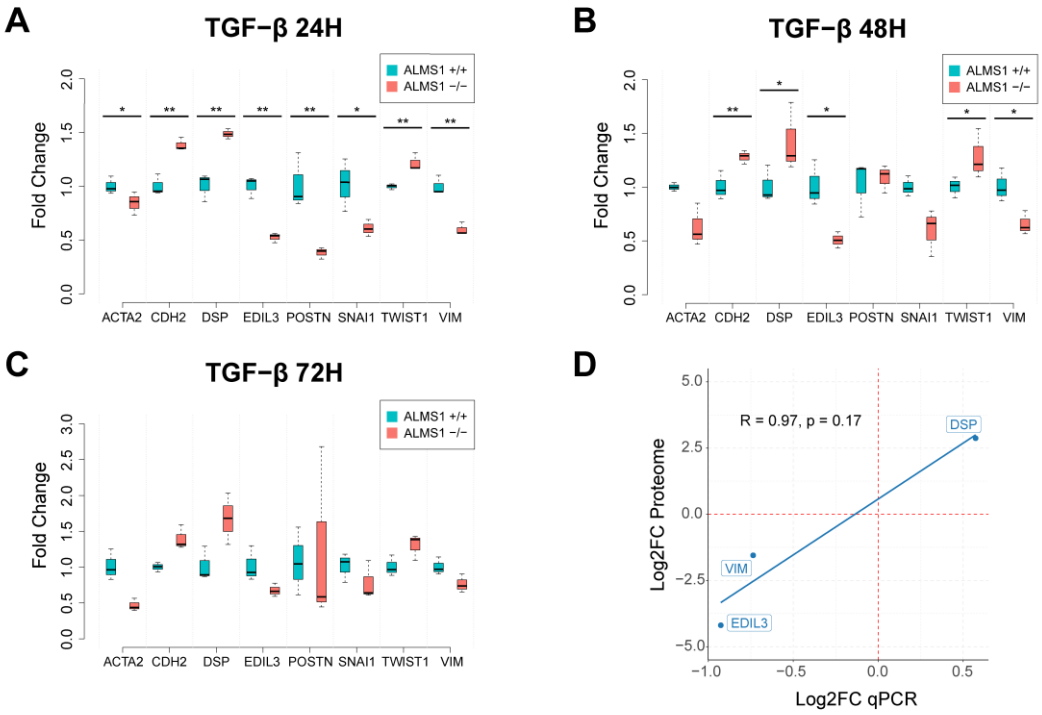

Figure 5. Expression validation of different EMT biomarkers with TGF-β stimulation at **(A)** 24 hours, **(B)** 48 hours, and **(C)** 72 hours. **(D)** Correlation plot between the expression of three EMT markers in the proteomic analysis and the qPCR assay. The expression is represented based on the log2 FC and the R coefficient using Pearson's method. These experiments were performed by triplicate (n=3). *: adj. p-value < 0.05, **: adj. p-value < 0.01.

At 24 hours of stimulation, *POSTN*, *SNAI1*, *VIM, ACTA2* and *EDIL3* were found under-expressed, while *TWIST1*, *CDH2* and *DSP* were over-expressed (Figure 5.A). This data confirms the expression pattern previously detected in the proteome analysis related to the genes *VIM*, *DSP* and *EDIL3* (Figure 5.D).

At 48 hours of stimulation, the over-expressed genes *CDH2*, *TWIST1* and *DSP*, in addition to *EDIL3* and *VIM* inhibition, showed significant differences (Figure 5.B). The levels of the rest of the primary under-expressed genes were not significant.

Finally, at 72 hours of stimulation the expression pattern was similar to the previous stimulation times. However, the data dispersion was too high and no significant differences were detected.

The absence of *ALMS1* inhibits TGF-β/SMAD3/SNAI1 axis in hTERT BJ-5ta cell line and decreases migration capacity:

In order to validate the results obtained in the HeLa model, the TGF-β pathway was stimulated at 24 and 48 hours with the rh-TGF-β1 (2ng/µL) ligand on the CRISPR model in a hTERT BJ-5ta fibroblast line (Figure 6.A-B). In this cell line, inhibition of *VIM* and overexpression of *DSP* did not appear to occur. However, inhibition of *POSTN* and the transcription factor (TF) *SNAI1* seem to

204 be constant in both cell lines. *ACTA2* also showed decreased levels in BJ-5ta and HeLa but in the
205 latter, the difference was not too noticeable. Finally, we evaluated the SMAD3 phosphorilation
206 levels at 4 different times after TGF-β1 stimuli (0, 10, 30 and 90 min). We concluded that the
207 lack of *ALMS1* potentially inhibits the axis TGF-β/SMAD3/SNAI1 because phosphorylated SMAD3
208 levels appear to be reduced in BJ ALMS1 -/- cells (Figure 6 C,E). This could be affecting the normal
209 cell migration capacity in these cells (Figure 6 D,F).

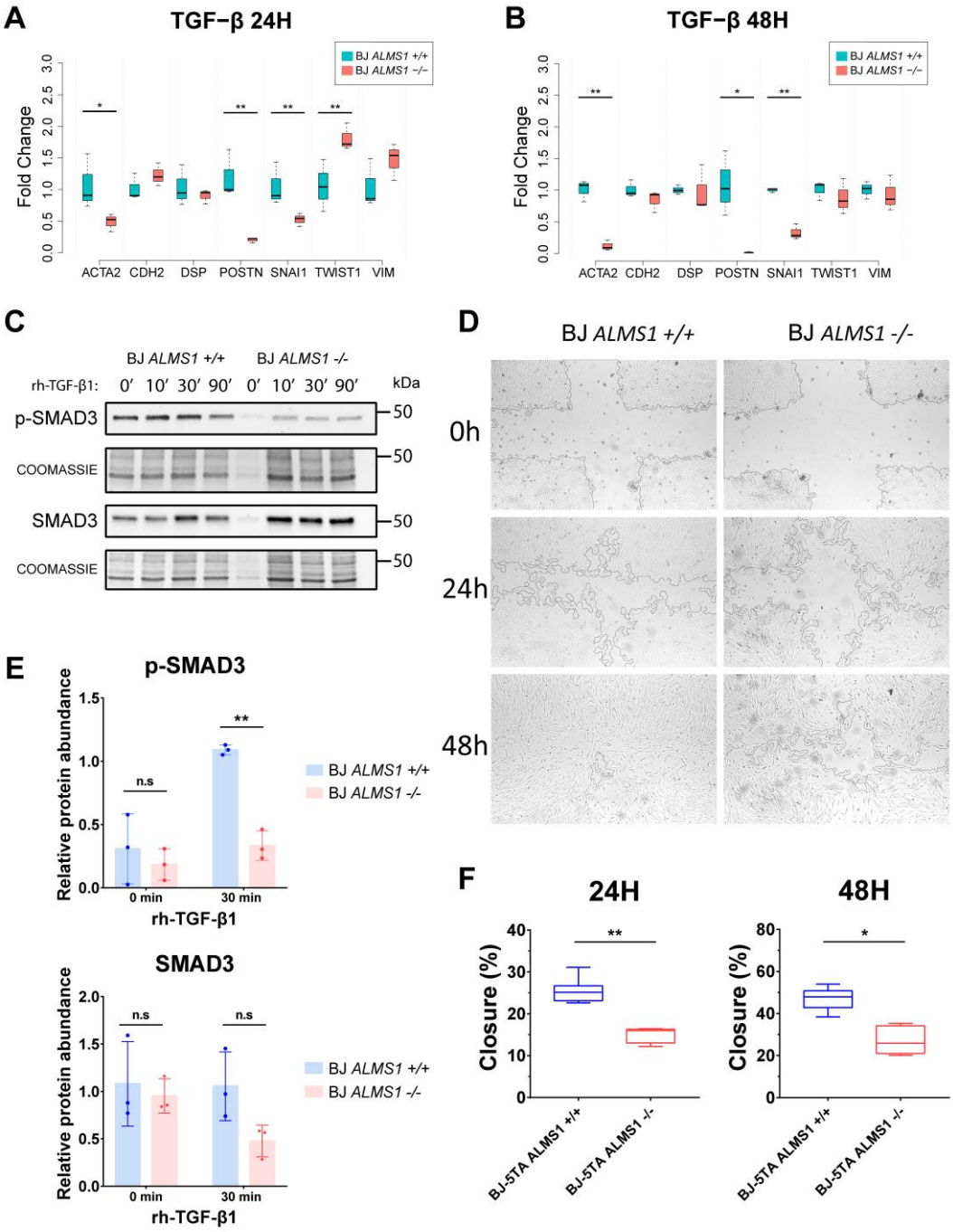

210

211

212 **Figure 6.** Expression levels of different EMT biomarkers, pSMAD3/SMAD3 and cell migration capacity in *ALMS1* -/- BJ-
213 5ta cell line. TGF-β stimulation was performed during 24 hours **(A)** and 48 hours **(B)** by triplicate (n=3). *: adj. p-value
214 < 0.05, **: adj. p-value < 0.01. **(C)** Representative western-blot of p-SMAD3 and SMAD3 levels after 0, 10, 20 and 90
215 min of stimulation with TGF-β1 (2 ng/µL) ligand and their corresponding loading controls (coomassie). **(D)**
216 Representative images of cell migration of BJ-5TA cells at 0, 24 and 48 hours in the presence of 2 ng/µL TGF-β1. **(E)**
217 Quantification of band intensity in WB for p-SMAD3 and SMAD3 at time 0 and after 30 min stimulation with TGF-β1.
218 (n=3). *: adj. p-value < 0.05, **: adj. p-value < 0.01. **(F)** Quantification of the cell area of the image and how it
219 decreased after 24 and 48 hours of incubation (n=3). *: p-value < 0.05, **: p-value < 0.01.

220 # DISCUSSION:

221 In this study, we reported new insights to understand the role of *ALMS1* in cell function. *ALMS1*
222 has a clear relation with cell cycle, apoptosis regulation, and cell migration and adhesion
223 processes such as EMT.

224 Cell cycle arrest in the G2/M phase (Figure 1. A-B), also described in *ALMS1*-knockdown
225 cardiomyocytes [23], seems to be a cell process triggered by *ALMS1* depletion. Several studies
226 have already linked cell cycle arrest in the G2/M phase to the TGF-β pathway and the
227 development of fibrosis [32]–[34]. This fact supports the involvement of the TGF-β pathway in
228 ALMS.

229 Normally, cell cycle arrest in both the G2/M and G0/G1 phases is often accompanied by the
230 activation of apoptotic processes [24], [35]–[37]. The depletion of *ALMS1* seems to generate
231 apoptosis resistance against THAP and C2-C in HeLa cells (Figure 2), which is in accordance with
232 that reported by Zulato et al., [8]. THAP is a non-competitive inhibitor for Ca^{2+}-ATPases located
233 in the endoplasmic reticulum (SERCA). This, inhibits Ca^{2+} reflux to the lumen of the endoplasmic
234 reticulum, generating endoplasmic reticulum stress (ER stress) [38]. At the same time, ER stress
235 activates a signalling network called Unfolded Protein Response (UPR) which alleviates this
236 stress and promotes cell survival, restoring ER homeostasis [39]. At this point, *ALMS1* depletion
237 could be acting at two levels: inhibiting THAP action (ER stress) or over-activating UPR and
238 generating apoptosis resistance. Because of the role of *ALMS1* in the centrosome and its relation
239 with endocytic trafficking [22], its depletion could probably alter the structure of the membrane,
240 inhibiting the signalling transduction of ligands like THAP. THAP also induces apoptosis impairing
241 cytoskeleton dynamics and disorganization of F-actin via mTORC1 inhibition in the mTORC1-
242 RhoA-Limk-Cofilin-1 axis in A549 cells [40]. *ALMS1* depletion already causes disorganization of
243 the F-actin cytoskeleton [22] but does not lead to cell death. Probably, the mTOR pathway
244 through mTORC1 was inhibited in *ALMS1* -/- cells, but in this case, other mechanisms could
245 prevent cells from reaching apoptotic stages. This would be supported by the inhibition of

246 LAMTOR3 (Figure 3.B), a protein involved in the formation of the Ragulator complex that
247 activates mTORC1 [41].

248 C2-C is a sphingolipid that induces caspases-dependent apoptosis, inhibiting PI3K/AKT pathway
249 and increasing the depolarisation of the mitochondrial membrane [42]–[44]. The over-activation
250 of the PI3K/AKT pathway could explain the apoptotic resistance in the case of the C2-C [45], [46].
251 This fact would agree with the previous proposed mTORC1 inhibition, since phosphorylation of
252 AKT/PKB at s473 leads to inhibition of mTORC1 mediated by FoxO transcription factors [47],
253 which could be related to F-actin filament disorganisation previously described in Alström
254 fibroblasts [22].

255 In addition to the role of *ALMS1* in G2/M phase cell cycle arrest and resistance to THAP- and C2-
256 C-mediated apoptosis, this study suggests that *ALMS1* depletion leads to inhibition of the
257 canonical (SMAD dependent) signalling pathway via the TGF-β. This could be affecting
258 downstream processes such as cell migration and EMT.

259 Our results show how the lack of *ALMS1* alters the expression of several genes related to focal
260 adhesion and cell-substrate adherens junction (Figure 4), two processes required for TGF-β1-
261 induced EMT [48], [49]. Moreover, we have found interesting candidates that could explain or
262 be related to the mentioned cellular disturbances (Figure 3). *S100A6*, under-expressed, is a
263 positive regulator of proliferation, migration and angiogenesis [50]–[52], and also a regulator of
264 endothelial calcium signaling [53]. *PKM*, which was over-expressed in HeLa cells, is associated
265 with apoptosis resistance [54]. *ITGA11*, another gene under-expressed in this cell line and
266 related to fibrosis generation, is expressed due to activation of the TGF-β pathway [55]. Finally,
267 two known EMT markers, *VIM* and *DSP*, showed a reverse pattern to that expected when this
268 process is activated. This could be a first evidence suggesting inhibition of the TGF-β1-induced
269 EMT when *ALMS1* is missing.

270 One of the most relevant detected genes was *SNAI1,* which is inhibited in both cell lines (Hela
271 and BJ-5ta). *SNAI1* and *TWIST1* are transcription factors that repress E-cadherin (*CDH1*)
272 expression and activate the expression of N-cadherins (*CDH2*) [56], [57]. E/N-cadherins switch is
273 involved in the induction of EMT [58], [59] through the TGF-β pathway [60]. Inhibition of *SNAI1*
274 could be affecting the normal EMT in these cells despite the over-expression of *TWIST1*. The
275 decreased expression of *SNAI1,* together with the inhibition of *ACTA2* and *POSTN,* also suggests
276 that TGF-β1-induced EMT would be down-regulated. *SNAI1* is up-regulated by SMAD3, which is
277 phosphorylated when the TGF-β pathway is activated and forms a complex with SMAD2 [17].
278 The phosphorylated SMAD2-SMAD3 complex translocates to the nucleus, activating the

expression of several genes related to cell migration and EMT such as *SNAI1* [61]. Because we detected consistent inhibition in both cell models, we sought to determine whether SMAD3 activation was also compromised in the BJ-5ta model. We conclude that *ALMS1* depletion inhibits SMAD3 phosphorylation (Figure 6 C, E), which could lead to downstream inhibition of *SNAI1* and affect migration capacity in this cell line (Figure 6 D,F), which could also affect the EMT.

We have previously described that *ALMS1* depletion by siRNA inhibits SMAD2 phosphorylation in the hTERT RPE-1 cell line [10]. This mechanism is probably also active in the HeLa and BJ-5ta cells and together with the inhibition of SMAD3 could explains the inhibition of *SNAI1* (Figure 5,6 A-B) through the TGF-β/SMAD3/SNAI1 axis [20]. This fact could be the main cause of the TGF-β pathway inhibition on the canonical part of the route, responsible for the expression pattern of the above-mentioned genes.

CONCLUSION:

ALMS1 appears to have a fairly conserved role in the regulation of cell cycle and apoptotic processes but does not affect mitochondrial reduction capacity. *ALMS1* depletion affects signal transduction through the canonical TGF-β pathway by inhibiting it. Inhibition of the TGF-β pathway would be affecting other downstream processes such as cell polarity control, EMT and migration capacity through the axis TGF-β/SMAD3/SNAI1.

MATERIALS AND METHODS:

Cell culture:

HeLa human cervical cancer cell line from American Type Culture Collection (ATCC), hTERT BJ-5ta human dermal fibroblasts (ATCC) and 293T human embryonic kidney cell line from ATCC were used. HeLa and 293T cells were maintained in Dulbecco's minimum essential medium (DMEM, Gibco, Invitrogen, NY, USA), supplemented with 10% fetal bovine serum (FBS) (Gibco, Invitrogen, NY, USA) and 2% penicillin/streptomycin (P/S) (Gibco, Invitrogen, NY, USA). In the case of BJ-5ta line, cells were maintained in DMEM:199, supplemented with 10% of FBS, 2% P/S and Hygromycin B (0.01mg/mL). All cell lines were grown at 37°C with 5% CO_2 for up to one month. After this, the cells were discarded and a new culture was started.

Crispr assay and edition validation:

HeLa cells were edited with a dual episomal system for homology directed repair (HDR) (Santa Cruz Biotechnology, Inc., Dallas, USA). Cells were transfected with Lipofectamine 2000 (Thermo Fisher, Waltham, EE. UU) using 3 gRNAs directed to *ALMS1* exons 1 and 3 (Supplementary Table S1). After plasmid transfection, cells were selected with puromycin (1 µg/mL) for 5 days.

Supplementary Table S1. gRNAs of the constructs used for gene editing. The forward and reverse sequences are shown in the table. The red colour represents the base pairs added for ligation in the plasmid.

ID	Cell line	Exon	Forward primer (gRNA sequence 5' - 3')	Reverse primer (5' - 3')	Strand	PAM	On-target Score	Off-Target Score
gRNA 1 HeLa	HeLa	1	GCCCCCGCAGCACCGCTACT	AGTAGCGGTGCTGCGGGGGC	+	CGG	51,4	89,3
gRNA 2 HeLa	HeLa	1	TCCGCTCGCCCTCCGAGTAG	CTACTCGGAGGGCGAGCGGA	-	CGG	56	91
gRNA 3 HeLa	HeLa	3	TTCTCACATTAAACCTAGTC	GACTAGGTTTAATGTGAGAA	-	TGG	29,1	76,7
gRNA 1 BJ	hTERT-BJ-5ta	3	CACCGCCTAGTCTGGGATGTATCCA	aaacTGGATACATCCCAGACTAGGCC	-	AGG	56,2	77,1
gRNA 2 BJ	hTERT-BJ-5ta	3	CACCGAACAGAAGAGATCTCTGTT	aaacAACAGAGATCTCTTCTGTTC	-	GGG	63,3	58,1

BJ-5ta cells were edited using a lentivirus system according to the protocol described by Sanjana et al [62], with some modifications. Check supplemental material for more information. After lentiviral transduction, cells were selected with puromycin (1µg/mL) for 5 days.

320 Surviving cells were expanded and isolated to obtain individual clones. Of the isolation was
321 performed using Fluorescence-Activated Cell Sorting (FACS) with Hoechst (BD Bioscience, San
322 José, USA) in the flow cytometer FACS ARIA III (BD Bioscience, San José, USA). Inhibition of gene
323 expression was validated by qPCR in a StepOnePlus instrument (Thermo Fisher, Waltham, USA).

324 Mitochondrial activity assay:

325 Mitochondrial activity was evaluated using Presto Blue reagent (Thermo Fisher, Waltham, USA).
326 Wild type (*ALMS1* +/+) and Hela Knockout cells (*ALMS1* -/-) were seeded in 96-well plates by
327 triplicate in concentrations from 5 x 10^4 to 1.5 x 10^3 cells per well. The plates were incubated for
328 24 hours as previously described. After incubation, 10 µL of Presto Blue were added to each well
329 and cells were incubated for 2 hours. Next, the plate was centrifuged at 1500 rpm for 5 min and
330 the supernatant was transferred to a fluorescence plate (Corning, NY, EE. UU). Finally, the plates
331 were measured in the Envision plate reader (Perkin-Elmer, Waltham, USA). This experiment was
332 repeated 3 times on different days.

333 Apoptosis assay:

334 The apoptosis assay was performed in flat-bottom 96-well plates. HeLa *ALMS1* +/+ and *ALMS1* -
335 /- cells were seeded in triplicate at a concentration of 3 x 10^4 cells/per well and incubated 24
336 hours before treatment. Next, apoptotic stimuli were added at the established concentrations,
337 followed by incubation for 24-48 hours depending on the stimuli. After that, cells were washed
338 twice with 100 µL PBS. 50 µL trypsin was added per well and the plate was incubated for 5 min
339 at 37°C. After that, trypsin was inactivated with 50 µL DMEM 10% FBS 2% P/S, and cells were
340 transferred to 96-well plates with U bottom. The plate was centrifugated at 1500 rpm for 5 min,
341 the supernatant was discarded and the cells were resuspended in 200 µL biding buffer with 2µL
342 7-AAD and 2µL annexin V-FITC (Biolegend Inc, San Diego, CA, USA). The plate was incubated for
343 15 min in darkness and measured in the flow cytometer FC 500 (Beckman-Coulter, Brea, CA,
344 USA). This experiment was repeated 3 times on different days.

345 Cell cycle assay:

346 To determine cell cycle alterations, we studied sub-populations in the HeLa *ALMS1* -/- model
347 with Hoechst staining (BD Bioscience, San José, USA). *ALMS1* +/+ and *ALMS1* -/- cells were
348 seeded in a 6-well plate at a concentration of 3 X 10^5 cells/per well and incubated overnight. The
349 next day, Hoechst staining was added to the medium and the plate was incubated for 1 hour.
350 Then, the medium was removed, cells were washed twice with 1 mL PBS per well,and trypsinised

351 following the protocol described above. Cells were resuspended in PBS and analysed in the flow
352 cytometer FACS ARIA III.

353 Protein extraction:

354 Cells were seeded in 6-well plates by triplicate in DMEM 2% P/S and incubated overnight for
355 serum starvation. One the next day, cells were stimulated with rh-TGF-β1 (2ng/mL; R&D
356 Systems) during 24 hours. After that, DMEM was removed and wells were washed twice with
357 PBS. Cells were scrapped in PBS. Then, cells were pelleted at 11000 rpm for 5 min, and 100 µL
358 of RIPA Buffer were added to each sample. Samples were incubated on ice for 20 min in constant
359 agitation. Finally, cell debris was pelleted by centrifugation for 30 min at 12000 rpm and 4 °C.
360 Samples were aliquoted and stored at -80 °C until the next protocol's step. Protein quantification
361 was performed by Bradford microplate assay (Bio-Rad, Hercules, USA).

362 Protein concentration, reduction and alkylation:

363 Initially, 20 µg of each sample was concentrated and stained with Coomassie in a 12% SDS-PAGE
364 gel. Bands were cut and faded. Band distinction was performed by adding 100 µL of ammonium
365 bicarbonate 25mM/50% acetonitrile and incubated 20 min. This step was repeated 4 times.
366 After distinction, the supernatant was removed and 100 µL of ammonium bicarbonate 25mM-
367 50% EtOH was added to samples, and incubated for 20 min. Then, the supernatant was removed
368 and 100 µL EtOH was added and incubated for 15 min. In the next step, 200 µL 10mM DTT in
369 ammonium bicarbonate were added and samples were incubated for 1 hour at 56°C. Then, DTT
370 solution was removed and 200 µL iodoacetamide (IAA) 55mM in 50 mM ammonium bicarbonate
371 was added. Samples were incubated again for 30 min at room temperature. Finally, the
372 supernatant was removed, 200 µL ammonium bicarbonate 50mM were added and samples
373 were incubated for 15 min.

374 Protein digestion:

375 After reduction and alkylation, samples were digested. 100 µL ammonium bicarbonate 25mM-
376 50% acetonitrile (ACN) was added to each sample and incubated for 30 min. The supernatant
377 was removed and 100 µL ACN 100% was added and incubated for 10 min. The supernatant was
378 removed again and 15 µL Trypsin in ammonium bicarbonate 25mM were added to each sample.
379 Samples were maintained at 4°C for 30 min. Finally, trypsin was removed, 5 µL ammonium
380 bicarbonate 25 mM were added and samples were incubated overnight.

381

382 ## Peptide extraction:

383 40 µL of trifluoroacetic acid (TFA) 0.5% were added to each sample and incubated for 30 min at
384 room temperature. Then, we added 20 µL ACN 100% in each 1.5 mL tube and incubated for 15
385 min at 37°C. Finally, the samples were dried in a speed-vac at 45°C for 1 hour and stored at -
386 20°C until the analysis.

387 ## Mass Spectrometry and bioinformatic analysis:

388 Samples were resuspended in 24 µL formic acid 0.1%. Then, 10 µL were injected into the HPLC
389 (LC-ESI-MS/MS workflow using a C18 precolumn). Samples were analysed in a mass
390 spectrophotometry Orbitrap ELITE (Thermo-Fisher, Waltham, USA) in long chromatography
391 mode (4 hours). After that, protein identification was performed in the database
392 UniProtKB/TrEMBL for humans, using the Proteome Discoverer software. Downstream analysis
393 was performed with the R package Differential Enrichment analysis of Proteomics data (DEP
394 package) [63]. Finally, Go Terms analysis was performed with Clusterprofiler package [64], and
395 results were visualized with GOplot package [65]. All the code for the analysis was deposited in
396 the GitHub repository (https://github.com/BreisOne/CRISPR_Hela_KO_Alms1).

397 The mass spectrometry proteomics data have been deposited in the ProteomeXchange
398 Consortium via the PRIDE [66] partner repository with the dataset identifier PXD024964.

399 ## RNA extraction and RT-PCR:

400 Cells were seeded in 6-well plates at a concentration of $2x10^5$ by triplicate in DMEM 2%P/S and
401 were incubated overnight for serum starvation. The next day, cells were stimulated with rh-TGF-
402 β1 (2 ng/mL) for 24, 48 and 72 hours. DMEM was removed and wells were washed twice with
403 PBS. Cells were scraped in PBS and collected in a 1.5 mL tubef. For the RNA extraction, the NYZ
404 total RNA isolation kit (NYZtech, Lisboa, Portugal) was used following the manufacture´s
405 protocol.

406 After RNA elution, the sample concentrations were measured with Nanodrop (Thermo Fisher,
407 Waltham, USA). Next, 300 ng of RNA were retrotranscribed to cDNA using the NZY First-Strand
408 cDNA Synthesis kit (NYZtech, Lisboa, Portugal) following the manufacture´s protocol.

409 ## qPCR expression analysis:

410 qPCRs was performed in a StepOnePlus instrument using SyBr green (Thermo Fisher, Waltham,
411 EE. UU). Primers were synthesized on demand (IDT) (Supplementary Table S2). Samples were
412 analysed by technical triplicates for each sample and gene. Cts for technical triplicates were

413 averaged using the geometric mean and ΔΔCT method was applied for the normalization, using
414 2 housekeeping (HK) genes (*ALAS1* and *YWHATZ*).

415 **Supplementary Table S2.** Sequences of the primers used for the evaluation of qPCR expression of
416 epithelial-mesenchymal transition markers and genotyping of the HeLa Knockout line.

Gene symbol	Forward primer	Reverse primer
POSTN	CACTCTTTGCTCCCACCAAT	GCCACTTTGTCTCCCATGAT
CDH2	CCTCCAGAGTTTACTGCCATGAC	GTAGGATCTCCGCCACTGATTC
ACTA2	CTATGCCTCTGGACGCACAACT	CAGATCCAGACGCATGATGGCA
SNAI1	GCTGCAGGACTCTAATCCAGAGTT	GACAGAGTCCCAGATGAGCATTG
TWIST1	GCCAGGTACATCGACTTCCTCT	TCCATCCTCCAGACCGAGAAGG
EDIL3	GCGAATGGAACTTCTTGGCTGTG	GAGCGTTCTGAAGATGCTGGAG
VIM	AGGCAAAGCAGGAGTCCACTGA	ATCTGGCGTTCCAGGGACTCAT
DSP	TGACAGACCGCTGGCAAAGGAT	GGCGTTTAGCATCATAGAGCCAC
ALMS1 (Exon1)	GCACTGCGCCTAAGCTG	gttgggggtggaggctg
ALMS1 (Exon3)	cagttaatgacttagcatgttttcct	ctttccccttttgagttaagga
ALMS1 (Exon 1 -3)	GAGCGAGACACCAACATGGA	ATTGCGTCAATATGCCCTCCT

417

418 Wound healing assay:

419 BJ-5ta ALMS1 +/+ and ALMS1 -/- were seeded by triplicate in a 6-well plate at a concentration
420 of $1x10^6$ and cultured until a 90-95% of confluence. Cells were serum-starvated for 24 hours.
421 After that, TGF-β1 (2 ng/mL) was added to all wells and a wound performed with a 200 µL pipette
422 tip. Cells were incubated at 37°C 5% CO_2 and images were taken at 0, 24 and 48 hours with the
423 microscope inverted Nikon TiU. Finally, images were analysed with the imageJ program [67] and
424 the plugin developed by Suarez-Armendo et al [68].

425 Western-Blot:

426 Samples were collected from 6-well plates and lysed in RIPA buffer, containing phosphatase
427 inhibitors (dil 1:200) and protease inhibitors (1:1000), for 30min at 4ºC. Then samples were
428 centrifugated during 20min at 12000 rpms and 4ºC. The supernatant was collected to 1.5mL low
429 binding tubes and pellet was discarded. Quantification was performed using Bradford assay in
430 microplates. Samples were stored at -80°C until analysis.

431 A total amount of 20µg from each sample were mixed with 6,25µL of Laemmli Buffer 4X (Biorad,
432 Hércules, EE.UU), 1,25µL β-mercaptoethanol (BME) and a volume of H_2O_d up to a final volume
433 of 25µL. Then, the mixes were boiled at 97ºC for 5 min and loaded in a Mini-PROTEAN® TGX™
434 Precast Gel (Biorad, Hércules, EE.UU) at 12% acrylamide/bis-acrylamide. The gel was migrated
435 for 1 hour at 150V. Then, gels were transferred to a 0.2 µm PVDF membrane using the Trans-

436 Blot Turbo transfer system (Biorad, Hércules, EE.UU) following the mixed molecular weight
437 (MW) protocol. After transfer, membranes were blocked with in-house tris-buffered saline, 0.1%
438 Tween20 and 5% milk (TBS-T 5%) for 90 min. Incubation with the primary antibody was kept at
439 4°C overnight. The primary antibodies used in this assay were: anti-SMAD3 (1:1000,
440 Abcam,40854) and anti-p-SMAD3 (1:1000, Abcam, 63403).

441 Next day, incubation with secondary antibody was performed by 45min in TBST 5%, after
442 washed the membrane 3 times in TBST 5%. The secondary antibody used in this assay was goat
443 anti-rabbit IgG H&L (HRP) (Abcam, 205718) at 1:5000 for p-SMAD3 and 1:15000 for SMAD3.
444 Finally, for protein visualization Clarity western ECL substrate (Biorad, Hércules, EE.UU) was used
445 and membranes were exposed in the ChemiDoc system (Biorad, Hércules, EE.UU).
446 Quantification of protein bands was carried on Image Lab software (Biorad, Hércules, EE.UU)
447 using the total protein standardisation method.

448 Statistical analysis:

449 On one hand, mitochondrial activity, apoptosis and cell cycle data visualization and statistical
450 analysis were performed with the software GraphPad Prism 7.00.

451 Mitochondrial activity was analysed using a linear regression model. Comparison of fluorescence
452 increase with cell concentration did not show significant differences between both slopes (α =
453 0.05). The apoptosis experiment results were analysed with 2ways-Anova to compare each
454 different population between genotypes. A Sidak's multiple comparisons test was applied to
455 correct the analysis. Finally, cell cycle results were analysed with a two-tailed unpaired t-test for
456 each population (G2/M, S and G0/G1).

457 On the other hand, proteomic data analysis included different statistical analyses and data
458 transformations along the pipeline. Initially, the data were normalised by variance stabilizing
459 transformation (VSN). The data imputation for missing values was performed like missing not at
460 random (MNAR) using the Minprob method with FDR < 0.01. Finally, differential expression
461 analysis was performed using protein-wise linear models combined with empirical Bayes
462 statistics implemented in the limma package, FDR < 0.05.

463 A third analysis was performed for the qPCR data. After normalization, fold changes (FC) were
464 calculated concerning the geometric mean of the expression of each gene in the biological
465 triplicates for *ALMS1* +/+. Significant differences were calculates using a multiple t-test with a
466 significant threshold of FDR < 0.05.

467 Finally western-blot data were normalized using total protein method. After normalization FCs
468 were calculated using the geometric mean of the expression/activation of the protein in each
469 clone. Significant differences were calculates using a multiple t-test with a significant threshold
470 of FDR < 0.05. For wound healing assay, an unpaired t-test was applied and a significant
471 threshold of p-value <0.05 was set.

472 **Author Contributions:** BB-M and DV designed the study. BB-M performed the experiments and
473 analysed the data. EN-G assisted in performing apoptosis, cell cycle and mitochondrial activity
474 assays. AI-R assisted in the quantification of the expression of EMT markers in the BJ-5ta model
475 and in the cell migration assay. BB-M and DV wrote the manuscript. All authors have read the
476 draft and provided approval for publication.

477 **Data Availability Statement:** Proteomic data are available via ProteomeXchange with identifier
478 PXD024964.

479 **Acknowledgments:** We sincerely thank the Proteomics and Genomics services from Centro de
480 Apoyo Científico-Tecnológico a la Investigación (CACTI) of University of Vigo and its specialists
481 Paula Álvarez Chaver, Ángel Sebastián Comesaña, Verónica Outeiriño and Manuel Marcos for
482 their guidance and advise. We also thank Mercedes Peleteiro Olmedo from Centro de
483 Investigacións Biomédicas (CINBIO) from University of Vigo for the flow cytometry service.

484 **Funding:** This work was funded by Instituto de Salud Carlos III (project PI15/00049 and
485 PI19/00332), Xunta de Galicia (Centro de Investigación de Galicia CINBIO 2019-2022; Ref.
486 ED431G-2019/06) and Consolidación e estructuración de unidades de investigación
487 competitivas e outras accións de fomento (Xunta de Galicia, ED431C-2018/54). Brais Bea-
488 Mascato (FPU17/01567) was supported by graduate studentship awards (FPU predoctoral
489 fellowship) from the Spanish Ministry of Education, Culture and Sports.

490 **Conflicts of Interest:** The authors declare no conflict of interest. The funders had no role in the
491 design of the study; in the collection, analyses, or interpretation of data; in the writing of the
492 manuscript, or in the decision to publish the results.

493

494 # BIBLIOGRAPHY:

495 [1] J. D. Marshall, P. Maffei, G. B. Collin, and J. K. Naggert, “Alström syndrome: genetics and
496 clinical overview,” *Curr. Genomics*, vol. 12, no. 3, pp. 225–235, May 2011, doi:
497 10.2174/138920211795677912.

498 [2] A. B. Jaykumar, P. Caceres, E. L. Henson, W. H. Beierwaltes, and P. A. Ortiz, “Deletion of
499 ALMS1 (Alstrom Syndrome 1) enhances salt-sensitive hypertension, and induces insulin
500 resistance and obesity in rats.,” *FASEB J.*, vol. 31, no. 1_supplement, pp. 857.26-857.26,
501 Apr. 2017, doi: 10.1096/fasebj.31.1_supplement.857.26.

502 [3] G. B. Collin *et al.*, “Mutations in ALMS1 cause obesity, type 2 diabetes and neurosensory
503 degeneration in Alström syndrome,” *Nat. Genet.*, vol. 31, p. 74, Apr. 2002, [Online].
504 Available: https://doi.org/10.1038/ng867.

505 [4] J. D. Marshall *et al.*, “Spectrum of ALMS1 variants and evaluation of genotype-phenotype
506 correlations in Alström syndrome,” *Hum. Mutat.*, vol. 28, no. 11, pp. 1114–1123, Nov.
507 2007, doi: 10.1002/humu.20577.

508 [5] T. Hearn *et al.*, “Subcellular Localization of ALMS1 Supports Involvement of Centrosome
509 and Basal Body Dysfunction in the Pathogenesis of Obesity, Insulin Resistance, and Type
510 2 Diabetes,” *Diabetes*, vol. 54, no. 5, pp. 1581 LP – 1587, May 2005, doi:
511 10.2337/diabetes.54.5.1581.

512 [6] D. Jagger *et al.*, “Alström Syndrome protein ALMS1 localizes to basal bodies of cochlear
513 hair cells and regulates cilium-dependent planar cell polarity.,” *Hum. Mol. Genet.*, vol.
514 20, no. 3, pp. 466–481, Feb. 2011, doi: 10.1093/hmg/ddq493.

515 [7] G. Li *et al.*, “A role for Alström syndrome protein, alms1, in kidney ciliogenesis and cellular
516 quiescence,” *PLoS Genet.*, vol. 3, no. 1, pp. e8–e8, Jan. 2007, doi:
517 10.1371/journal.pgen.0030008.

518 [8] E. Zulato *et al.*, “ALMS1-deficient fibroblasts over-express extra-cellular matrix
519 components, display cell cycle delay and are resistant to apoptosis,” *PLoS One*, vol. 6, no.
520 4, pp. e19081–e19081, Apr. 2011, doi: 10.1371/journal.pone.0019081.

521 [9] C. C. Leitch, S. Lodh, V. Prieto-Echagüe, J. L. Badano, and N. A. Zaghloul, “Basal body
522 proteins regulate Notch signaling through endosomal trafficking.,” *J. Cell Sci.*, vol. 127,
523 no. Pt 11, pp. 2407–2419, Jun. 2014, doi: 10.1242/jcs.130344.

524 [10] M. Álvarez-Satta *et al.*, "ALMS1 Regulates TGF-β Signaling and Morphology of Primary
525 Cilia," *Frontiers in Cell and Developmental Biology*, vol. 9, p. 112, 2021.

526 [11] A. B. Roberts *et al.*, "Smad3 is key to TGF-β-mediated epithelial-to-mesenchymal
527 transition, fibrosis, tumor suppression and metastasis," *Cytokine Growth Factor Rev.*, vol.
528 17, no. 1–2, pp. 19–27, Feb. 2006, doi: 10.1016/J.CYTOGFR.2005.09.008.

529 [12] W. KL, J. KE, and H. CA, "Targeting TGF-β Mediated SMAD Signaling for the Prevention of
530 Fibrosis," *Front. Pharmacol.*, vol. 8, no. JUL, Jul. 2017, doi: 10.3389/FPHAR.2017.00461.

531 [13] C. A. Clement *et al.*, "TGF-β Signaling Is Associated with Endocytosis at the Pocket Region
532 of the Primary Cilium," *Cell Rep.*, vol. 3, no. 6, pp. 1806–1814, 2013, doi:
533 https://doi.org/10.1016/j.celrep.2013.05.020.

534 [14] Y. Zhang, P. B. Alexander, and X. F. Wang, "TGF-β family signaling in the control of cell
535 proliferation and survival," *Cold Spring Harb. Perspect. Biol.*, vol. 9, no. 4, Apr. 2017, doi:
536 10.1101/cshperspect.a022145.

537 [15] L. K, "Signaling Cross Talk between TGF-β/Smad and Other Signaling Pathways," *Cold*
538 *Spring Harb. Perspect. Biol.*, vol. 9, no. 1, Jan. 2017, doi: 10.1101/CSHPERSPECT.A022137.

539 [16] J. Massagué, "TGFβ signalling in context," *Nature Reviews Molecular Cell Biology*, vol. 13,
540 no. 10. NIH Public Access, pp. 616–630, Oct. 2012, doi: 10.1038/nrm3434.

541 [17] A. Nakao *et al.*, "TGF-β receptor-mediated signalling through Smad2, Smad3 and Smad4,"
542 *EMBO J.*, vol. 16, no. 17, pp. 5353–5362, Sep. 1997, doi: 10.1093/EMBOJ/16.17.5353.

543 [18] S. Thuault, E.-J. Tan, H. Peinado, A. Cano, C.-H. Heldin, and A. Moustakas, "HMGA2 and
544 Smads Co-regulate SNAIL1 Expression during Induction of Epithelial-to-Mesenchymal
545 Transition," *J. Biol. Chem.*, vol. 283, no. 48, p. 33437, Nov. 2008, doi:
546 10.1074/JBC.M802016200.

547 [19] Y. Wang, J. Shi, K. Chai, X. Ying, and B. P. Zhou, "The Role of Snail in EMT and
548 Tumorigenesis."

549 [20] T. Vincent *et al.*, "A SNAIL1-SMAD3/4 transcriptional repressor complex promotes TGF-β
550 mediated epithelial-mesenchymal transition," *Nat. Cell Biol.*, vol. 11, no. 8, pp. 943–950,
551 2009, doi: 10.1038/ncb1905.

552 [21] X. Yan *et al.*, "Smad7 Protein Interacts with Receptor-regulated Smads (R-Smads) to
553 Inhibit Transforming Growth Factor-β (TGF-β)/Smad Signaling *," *J. Biol. Chem.*, vol. 291,

554 no. 1, pp. 382–392, Jan. 2016, doi: 10.1074/JBC.M115.694281.

555 [22] G. B. Collin *et al.*, “The Alström syndrome protein, ALMS1, interacts with α-actinin and
556 components of the endosome recycling pathway,” *PLoS One*, vol. 7, no. 5, pp. e37925–
557 e37925, 2012, doi: 10.1371/journal.pone.0037925.

558 [23] L. T. Shenje *et al.*, “Mutations in Alström protein impair terminal differentiation of
559 cardiomyocytes,” *Nat. Commun.*, vol. 5, p. 3416, Mar. 2014, doi: 10.1038/ncomms4416.

560 [24] R. Horbay and R. Bilyy, “Mitochondrial dynamics during cell cycling,” *Apoptosis*, vol. 21,
561 no. 12. Springer New York LLC, pp. 1327–1335, Dec. 01, 2016, doi: 10.1007/s10495-016-
562 1295-5.

563 [25] M. H. Fox, “A model for the computer analysis of synchronous DNA distributions obtained
564 by flow cytometry.,” *Cytometry*, vol. 1, no. 1, pp. 71–77, Jul. 1980, doi:
565 10.1002/cyto.990010114.

566 [26] L. M. Westrate, A. D. Sayfie, D. M. Burgenske, and J. P. MacKeigan, “Persistent
567 mitochondrial hyperfusion promotes G2/M accumulation and caspase-dependent cell
568 death,” *PLoS One*, vol. 9, no. 3, p. 91911, Mar. 2014, doi: 10.1371/journal.pone.0091911.

569 [27] D. Arita, M. Kambe, C. Ishioka, and R. Kanamaru, “Induction of p53-independent
570 apoptosis associated with G2M arrest following DNA damage in human colon cancer cell
571 lines,” *Japanese J. Cancer Res.*, vol. 88, no. 1, pp. 39–43, Jan. 1997, doi: 10.1111/j.1349-
572 7006.1997.tb00299.x.

573 [28] I. Yoshida, A. Monji, K. Tashiro, K. Nakamura, R. Inoue, and S. Kanba, “Depletion of
574 intracellular Ca2+ store itself may be a major factor in thapsigargin-induced ER stress and
575 apoptosis in PC12 cells,” *Neurochem. Int.*, vol. 48, no. 8, pp. 696–702, 2006, doi:
576 https://doi.org/10.1016/j.neuint.2005.12.012.

577 [29] S. T. Christensen, S. K. Morthorst, J. B. Mogensen, and L. B. Pedersen, “Primary cilia and
578 coordination of receptor tyrosine kinase (RTK) and transforming growth factor β (TGF-β)
579 signaling,” *Cold Spring Harbor Perspectives in Biology*, vol. 9, no. 6. Cold Spring Harbor
580 Laboratory Press, p. a028167, Jun. 01, 2017, doi: 10.1101/cshperspect.a028167.

581 [30] F. Cheng *et al.*, “Vimentin coordinates fibroblast proliferation and keratinocyte
582 differentiation in wound healing via TGF-β-Slug signaling,” *Proc. Natl. Acad. Sci. U. S. A.*,
583 vol. 113, no. 30, pp. E4320–E4327, Jul. 2016, doi: 10.1073/pnas.1519197113.

584 [31] S. J. Serrano-Gomez, M. Maziveyi, and S. K. Alahari, “Regulation of epithelial-

585 mesenchymal transition through epigenetic and post-translational modifications," *Mol.*
586 *Cancer*, vol. 15, p. 18, Feb. 2016, doi: 10.1186/s12943-016-0502-x.

587 [32] L. Yang, T. Y. Besschetnova, C. R. Brooks, J. V Shah, and J. V Bonventre, "Epithelial cell
588 cycle arrest in G2/M mediates kidney fibrosis after injury," *Nat. Med.*, vol. 16, no. 5, pp.
589 535–543, 2010, doi: 10.1038/nm.2144.

590 [33] T. L. White, N. Deshpande, V. Kumar, A. G. Gauthier, and U. V Jurkunas, "Cell cycle re-
591 entry and arrest in G2/M phase induces senescence and fibrosis in Fuchs Endothelial
592 Corneal Dystrophy.," *Free Radic. Biol. Med.*, vol. 164, pp. 34–43, Feb. 2021, doi:
593 10.1016/j.freeradbiomed.2020.12.445.

594 [34] H. Li *et al.*, "Atg5-mediated autophagy deficiency in proximal tubules promotes cell cycle
595 G2/M arrest and renal fibrosis.," *Autophagy*, vol. 12, no. 9, pp. 1472–1486, Sep. 2016,
596 doi: 10.1080/15548627.2016.1190071.

597 [35] J. JAKUBIKOVA, Y. BAO, and J. SEDLAK, "Isothiocyanates Induce Cell Cycle Arrest,
598 Apoptosis and Mitochondrial Potential Depolarization in HL-60 and Multidrug-resistant
599 Cell Lines," *Anticancer Res.*, vol. 25, no. 5, 2005.

600 [36] N. B. Madungwe *et al.*, "Mitochondrial inner membrane protein (Mitofilin) knockdown
601 induces cell death by apoptosis via an AIF-PARP-dependent mechanism and cell cycle
602 arrest," *Am. J. Physiol. - Cell Physiol.*, vol. 315, no. 1, pp. C28–C43, Jul. 2018, doi:
603 10.1152/ajpcell.00230.2017.

604 [37] Y. Liu *et al.*, "Calycosin induces mitochondrial-dependent apoptosis and cell cycle arrest,
605 and inhibits cell migration through a ROS-mediated signaling pathway in HepG2
606 hepatocellular carcinoma cells," *Toxicol. Vitr.*, vol. 70, p. 105052, Feb. 2021, doi:
607 10.1016/j.tiv.2020.105052.

608 [38] P. Lindner, S. B. Christensen, P. Nissen, J. V. Møller, and N. Engedal, "Cell death induced
609 by the ER stressor thapsigargin involves death receptor 5, a non-autophagic function of
610 MAP1LC3B, and distinct contributions from unfolded protein response components," *Cell*
611 *Commun. Signal.*, vol. 18, no. 1, p. 12, 2020, doi: 10.1186/s12964-019-0499-z.

612 [39] C. M. Oslowski and F. Urano, "Measuring ER stress and the unfolded protein response
613 using mammalian tissue culture system," *Methods Enzymol.*, vol. 490, pp. 71–92, 2011,
614 doi: 10.1016/B978-0-12-385114-7.00004-0.

615 [40] F. Wang *et al.*, "Thapsigargin Induces Apoptosis by Impairing Cytoskeleton Dynamics in

616 Human Lung Adenocarcinoma Cells," *Sci. World J.*, vol. 2014, p. 619050, 2014, doi:
617 10.1155/2014/619050.

618 [41] Z. Mu, L. Wang, W. Deng, J. Wang, and G. Wu, "Structural insight into the Ragulator
619 complex which anchors mTORC1 to the lysosomal membrane," *Cell Discov.*, vol. 3, no. 1,
620 p. 17049, 2017, doi: 10.1038/celldisc.2017.49.

621 [42] M. J. Zinda, C. J. Vlahos, and M. T. Lai, "Ceramide Induces the Dephosphorylation and
622 Inhibition of Constitutively Activated Akt in PTEN Negative U87MG Cells," *Biochem.*
623 *Biophys. Res. Commun.*, vol. 280, no. 4, pp. 1107–1115, 2001, doi:
624 https://doi.org/10.1006/bbrc.2000.4248.

625 [43] R. M. Sánchez-Mora, H. Arboleda, and G. Arboleda, "PINK1 Overexpression Protects
626 Against C2-ceramide-Induced CAD Cell Death Through the PI3K/AKT Pathway," *J. Mol.*
627 *Neurosci.*, vol. 47, no. 3, pp. 582–594, 2012, doi: 10.1007/s12031-011-9687-z.

628 [44] A. S. Arora, B. J. Jones, T. C. Patel, S. F. Bronk, and G. J. Gores, "Ceramide induces
629 hepatocyte cell death through disruption of mitochondrial function in the rat,"
630 *Hepatology*, vol. 25, no. 4, pp. 958–963, Apr. 1997, doi:
631 https://doi.org/10.1002/hep.510250428.

632 [45] S.-J. Jeong *et al.*, "PI3K/AKT inhibition induces caspase-dependent apoptosis in HTLV-1-
633 transformed cells," *Virology*, vol. 370, no. 2, pp. 264–272, 2008, doi:
634 https://doi.org/10.1016/j.virol.2007.09.003.

635 [46] B. N. Fahy, M. Schlieman, S. Virudachalam, and R. J. Bold, "AKT inhibition is associated
636 with chemosensitisation in the pancreatic cancer cell line MIA-PaCa-2," *Br. J. Cancer*, vol.
637 89, no. 2, pp. 391–397, 2003, doi: 10.1038/sj.bjc.6601037.

638 [47] C.-C. Chen *et al.*, "FoxOs Inhibit mTORC1 and Activate Akt by Inducing the Expression of
639 Sestrin3 and Rictor," *Dev. Cell*, vol. 18, no. 4, pp. 592–604, 2010, doi:
640 https://doi.org/10.1016/j.devcel.2010.03.008.

641 [48] C. Cicchini *et al.*, "TGFβ-induced EMT requires focal adhesion kinase (FAK) signaling," *Exp.*
642 *Cell Res.*, vol. 314, no. 1, pp. 143–152, 2008, doi:
643 https://doi.org/10.1016/j.yexcr.2007.09.005.

644 [49] T. Baronsky *et al.*, "Cell-Substrate Dynamics of the Epithelial-to-Mesenchymal
645 Transition.," *Nano Lett.*, vol. 17, no. 5, pp. 3320–3326, May 2017, doi:
646 10.1021/acs.nanolett.7b01558.

647 [50] A. Li *et al.*, “S100A6 promotes the proliferation and migration of cervical cancer cells via
648 the PI3K/Akt signaling pathway.,” *Oncol. Lett.*, vol. 15, no. 4, pp. 5685–5693, Apr. 2018,
649 doi: 10.3892/ol.2018.8018.

650 [51] A. Li *et al.*, “S100A6 promotes cell proliferation in human nasopharyngeal carcinoma via
651 the p38/MAPK signaling pathway.,” *Mol. Carcinog.*, vol. 56, no. 3, pp. 972–984, Mar.
652 2017, doi: 10.1002/mc.22563.

653 [52] P. Li, X. Lv, Z. Zhang, and S. Xie, “S100A6/miR193a regulates the proliferation, invasion,
654 migration and angiogenesis of lung cancer cells through the P53 acetylation.,” *Am. J.*
655 *Transl. Res.*, vol. 11, no. 8, pp. 4634–4649, 2019.

656 [53] B. Haldar *et al.*, “S100A6 is a positive regulator of PPP5C-FKBP51-dependent regulation
657 of endothelial calcium signaling.,” *FASEB J. Off. Publ. Fed. Am. Soc. Exp. Biol.*, vol. 34,
658 no. 2, pp. 3179–3196, Feb. 2020, doi: 10.1096/fj.201901777R.

659 [54] S. Calabretta *et al.*, “Modulation of PKM alternative splicing by PTBP1 promotes
660 gemcitabine resistance in pancreatic cancer cells.,” *Oncogene*, vol. 35, no. 16, pp. 2031–
661 2039, Apr. 2016, doi: 10.1038/onc.2015.270.

662 [55] N. Lu, S. Carracedo, J. Ranta, R. Heuchel, R. Soininen, and D. Gullberg, “The human α11
663 integrin promoter drives fibroblast-restricted expression in vivo and is regulated by TGF-
664 β1 in a Smad- and Sp1-dependent manner,” *Matrix Biol.*, vol. 29, no. 3, pp. 166–176, Apr.
665 2010, doi: 10.1016/j.matbio.2009.11.003.

666 [56] W. Jiao, K. Miyazaki, and Y. Kitajima, “Inverse correlation between E-cadherin and Snail
667 expression in hepatocellular carcinoma cell lines in vitro and in vivo,” *Br. J. Cancer*, vol.
668 86, no. 1, pp. 98–101, 2002, doi: 10.1038/sj.bjc.6600017.

669 [57] I. Poser, D. Domínguez, A. G. de Herreros, A. Varnai, R. Buettner, and A. K. Bosserhoff,
670 “Loss of E-cadherin Expression in Melanoma Cells Involves Up-regulation of the
671 Transcriptional Repressor Snail*,” *J. Biol. Chem.*, vol. 276, no. 27, pp. 24661–24666, 2001,
672 doi: https://doi.org/10.1074/jbc.M011224200.

673 [58] L. Hao, J. R. Ha, P. Kuzel, E. Garcia, and S. Persad, “Cadherin switch from E- to N-cadherin
674 in melanoma progression is regulated by the PI3K/PTEN pathway through Twist and
675 Snail,” *Br. J. Dermatol.*, vol. 166, no. 6, pp. 1184–1197, Jun. 2012, doi:
676 https://doi.org/10.1111/j.1365-2133.2012.10824.x.

677 [59] K. Gravdal, O. J. Halvorsen, S. A. Haukaas, and L. A. Akslen, “A Switch from E-Cadherin to

678 N-Cadherin Expression Indicates Epithelial to Mesenchymal Transition and Is of Strong
679 and Independent Importance for the Progress of Prostate Cancer," *Clin. Cancer Res.*, vol.
680 13, no. 23, pp. 7003 LP – 7011, Dec. 2007, doi: 10.1158/1078-0432.CCR-07-1263.

681 [60] K. Araki *et al.*, "E/N-cadherin switch mediates cancer progression via TGF-β-induced
682 epithelial-to-mesenchymal transition in extrahepatic cholangiocarcinoma," *Br. J. Cancer*,
683 vol. 105, no. 12, pp. 1885–1893, 2011, doi: 10.1038/bjc.2011.452.

684 [61] A. B. Roberts *et al.*, "Smad3 is key to TGF-β-mediated epithelial-to-mesenchymal
685 transition, fibrosis, tumor suppression and metastasis," *Cytokine Growth Factor Rev.*, vol.
686 17, no. 1–2, pp. 19–27, 2006, doi: 10.1016/j.cytogfr.2005.09.008.

687 [62] N. E. Sanjana, O. Shalem, and F. Zhang, "Improved vectors and genome-wide libraries for
688 CRISPR screening," *Nat. Methods*, vol. 11, no. 8, pp. 783–784, 2014, doi:
689 10.1038/nmeth.3047.

690 [63] X. Zhang, A. H. Smits, G. B. van Tilburg, H. Ovaa, W. Huber, and M. Vermeulen,
691 "Proteome-wide identification of ubiquitin interactions using UbIA-MS.," *Nat. Protoc.*,
692 vol. 13, no. 3, pp. 530–550, Mar. 2018, doi: 10.1038/nprot.2017.147.

693 [64] G. Yu, L.-G. Wang, Y. Han, and Q.-Y. He, "clusterProfiler: an R package for comparing
694 biological themes among gene clusters," *OMICS*, vol. 16, no. 5, pp. 284–287, May 2012,
695 doi: 10.1089/omi.2011.0118.

696 [65] W. Walter, F. Sánchez-Cabo, and M. Ricote, "GOplot: an R package for visually combining
697 expression data with functional analysis.," *Bioinformatics*, vol. 31, no. 17, pp. 2912–2914,
698 Sep. 2015, doi: 10.1093/bioinformatics/btv300.

699 [66] Y. Perez-Riverol *et al.*, "The PRIDE database and related tools and resources in 2019:
700 improving support for quantification data.," *Nucleic Acids Res.*, vol. 47, no. D1, pp. D442–
701 D450, Jan. 2019, doi: 10.1093/nar/gky1106.

702 [67] C. A. Schneider, W. S. Rasband, and K. W. Eliceiri, "NIH Image to ImageJ: 25 years of image
703 analysis," *Nat. Methods 2012 97*, vol. 9, no. 7, pp. 671–675, Jun. 2012, doi:
704 10.1038/nmeth.2089.

705 [68] A. Suarez-Arnedo, F. T. Figueroa, C. Clavijo, P. Arbeláez, J. C. Cruz, and C. Muñoz-
706 Camargo, "An image J plugin for the high throughput image analysis of in vitro scratch
707 wound healing assays," *PLoS One*, vol. 15, no. 7, Jul. 2020, doi:
708 10.1371/JOURNAL.PONE.0232565.

Supplementary Material and Methods:

CRISPR plasmids construction:

Single guides RNAs (sgRNAs) for BJ-5ta model were designing using benchling to generate a deletion of 113pb in the exon 3 of *ALMS1* (ENSG00000116127). The 2 sgRNA (5'- CCTAGTCTGGGATGTATCCA – 3' and 5'- GAACAGAAGAGATCTCTGTT – 3') result from benchling were cloned into the plasmid lentiCRISPR v2 [1] following a modified protocol from that described by Shalem et al [2]. LentiCRISPR v2 was a gift from Feng Zhang (Addgene plasmid #52961). Initially, 12.5µL (5µg) of LentiCRISPR V2 were digested with 3µL Esp3I (BsmBI), 3µL FastAP and 6µL 10X FastDigest Buffer from Thermo Fisher. Final volume was set at 60µL. Plasmid digestion was checked by migration in an agarose gel at 1%.

sgRNAs were phosphorylated and annealed with its correspondent oligo mixing as follow: 1µL sgRNA (100µM), 1µL of its complement oligo, 2µL of 5X T4 Buffer (Canvax, Cordoba, Spain), 0.5 T4 PNK (NEB, Ipswich, EE.UU) and 5.5 µL distilled H_20 (H_2Od). Mix reaction was incubated at 37ºC for 30min and 95ºC for 5min. The samples were then left to stand at room temperature for 2 hours and diluted at 1:50, 1:100 and 1:200 ratios.

The unpurified digested plasmid was ligated with the diluted sgRNAs as follows: 0.5µL digested LentiCRISPR v2, 2µL diluted sgRNA, 1µL T4 DNA Ligase (Canvax, Cordoba, Spain), 4.5µL H_2Od. The mix was incubated at 37ºC by 30min.

Finally, Stable Competent E.coli (NEB, Ipswich, EE.UU) were transformed by thermal shock according to the manufactured protocol and incubated at 30ºC overnight. After that, construct validation was carried out using forward primer for U6 promotor (5'- GACTATCATATGCTTACCGT -3') and reverse sgRNA.

Plasmids Transfection and Lentivirus production:

293T were seeded in a concentration of $3x10^5$ into a 6-well plate and incubated overnight. Then, 293T cells were co-transfected with each CRISPR construct and the plasmids psPAX2 and pCMV-VSV-G [3] using lipofectamine 3000 (Thermo Fisher, Waltham, EE. UU). pCMV-VSV-G was a gift from Bob Weinberg (Addgene plasmid #8454) and psPAX2 was a gift from Didier Trono (Addgene plasmid #12260)

Initially, 7.5µL of lipofectamine 3000 were diluted in 125µL of Opti-MEM medium (Thermo Fisher, Waltham, EE. UU) by duplicate. Then a total amount of 5µg of ADN (1.6µL for each

739 plasmid) were diluted at 250µL Opti-MEM. After that, diluted DNA and diluted lipofectamine
740 were mixed in a 1:1 ratio, centrifugated at 1200rpm and incubated for 20min at room
741 temperature. Finally, the 250µL of mix were applied to the wells containing the cells.

742 The cells were incubated with the mixture for 24 hours. Then, the mixture was removed and the
743 cell was cultured for a further 72 hours for lentivirus production.

744 Lentiviral transduction:

745 After 72 hours of culturing 293T cells transfected for lentivirus production, the culture medium
746 was collected in 15 mL tubes and filtered through a 45µm filter (Sartorious,). In addition, a
747 solution of complete DMEM medium without P/S with polybrene was prepared at a dilution of
748 1:1000 (8µg/ml).

749 Then, 300µL lentiviral preparation were mixed with 200µL complete DMEM médium with
750 polybrene for each well. An additional 1 ml of DMEM with polybrene was added and the plates
751 were centrifuged at 800g for 30 minutes. This step was repeated one more time. After the
752 second centrifugation the mix with lentivirus was added again and the plates were incubated
753 for 24 hours. Finally, mix was removed and cells were allowed to settle for 48 hours in DMEM
754 médium. They were then selected with puromycin (1ng/mL) for 5 days.

755 Edition validation:

756 After puromycin selection, clonal isolation and expansion we checked the lack of *ALMS1* gene
757 by qPCR in StepOnePlus (Thermo Fisher, Waltham, EE. UU). Finally, we found that these cells
758 had the expected exon 3 deletion by PCR with resolution of samples on a 2% agarose gel and
759 followed by sanger sequencing.

760

Supplementary figures:

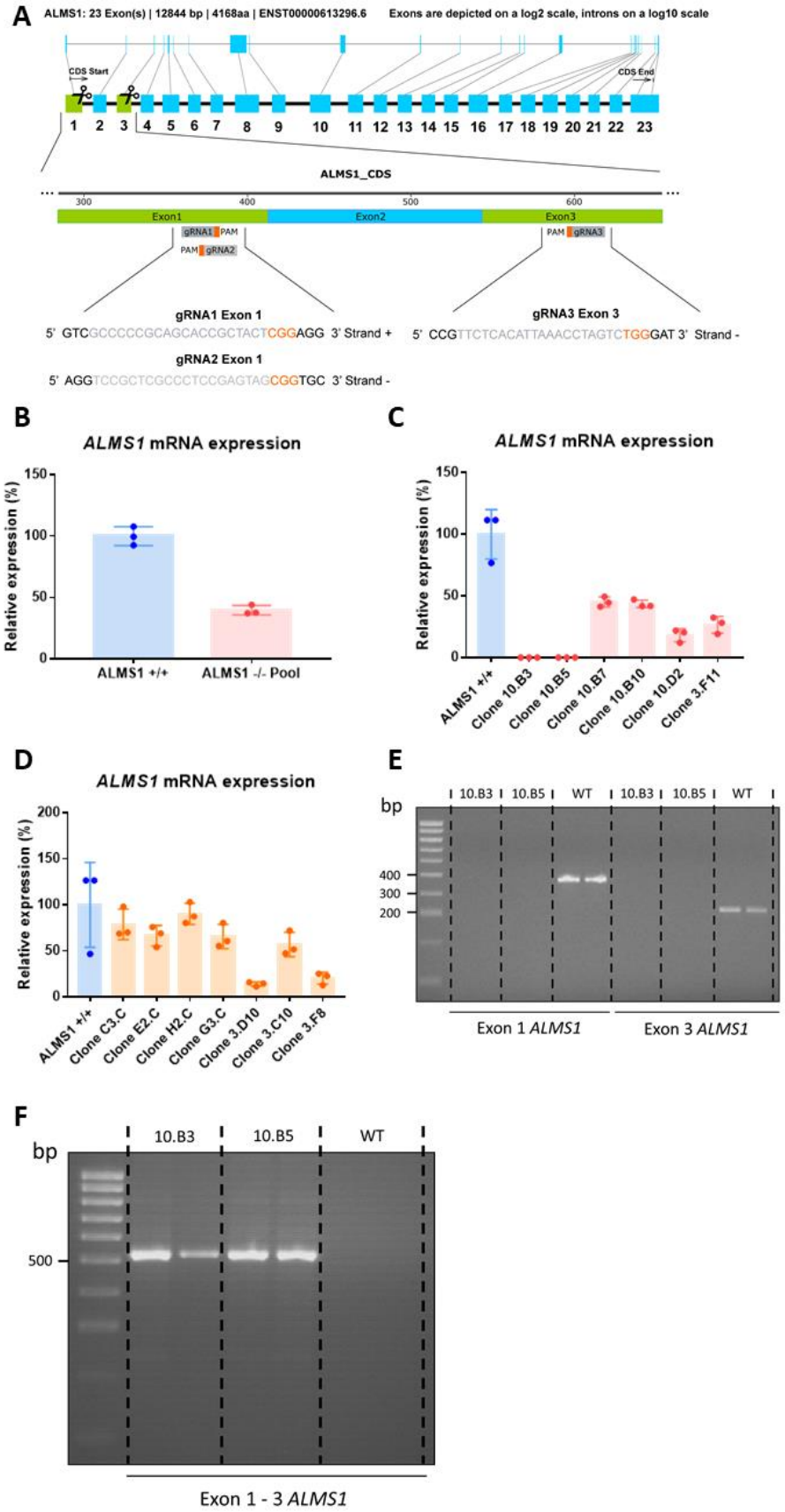

763 **Supplementary Figure S1.** Characterisation of *ALMS1* -/- cell line HeLa. **(A)** Design of the model.
764 **(B)** Relative gene expression of *ALMS1 +/+* and polyclonal cell line for *ALMS1 -/-* genotype. **(C)**
765 Relative gene expression of ALMS1 +/+ and a first batch of clones for *ALMS1 -/-* genotype. **(D)**
766 Relative gene expression of ALMS1 +/+ and second batch of clones for ALMS1 -/- genotype. **(E)**
767 Strategy for amplification of exons 1 and 3 from genomic DNA in two clones of the *ALMS1* -/-
768 (KO) line and the *ALMS1* +/+ control (WT). **(F)** Amplification strategy of the resulting sequence
769 between exon 1 and 3 after removal of the sequencing between the 2 outermost gRNAs.

770

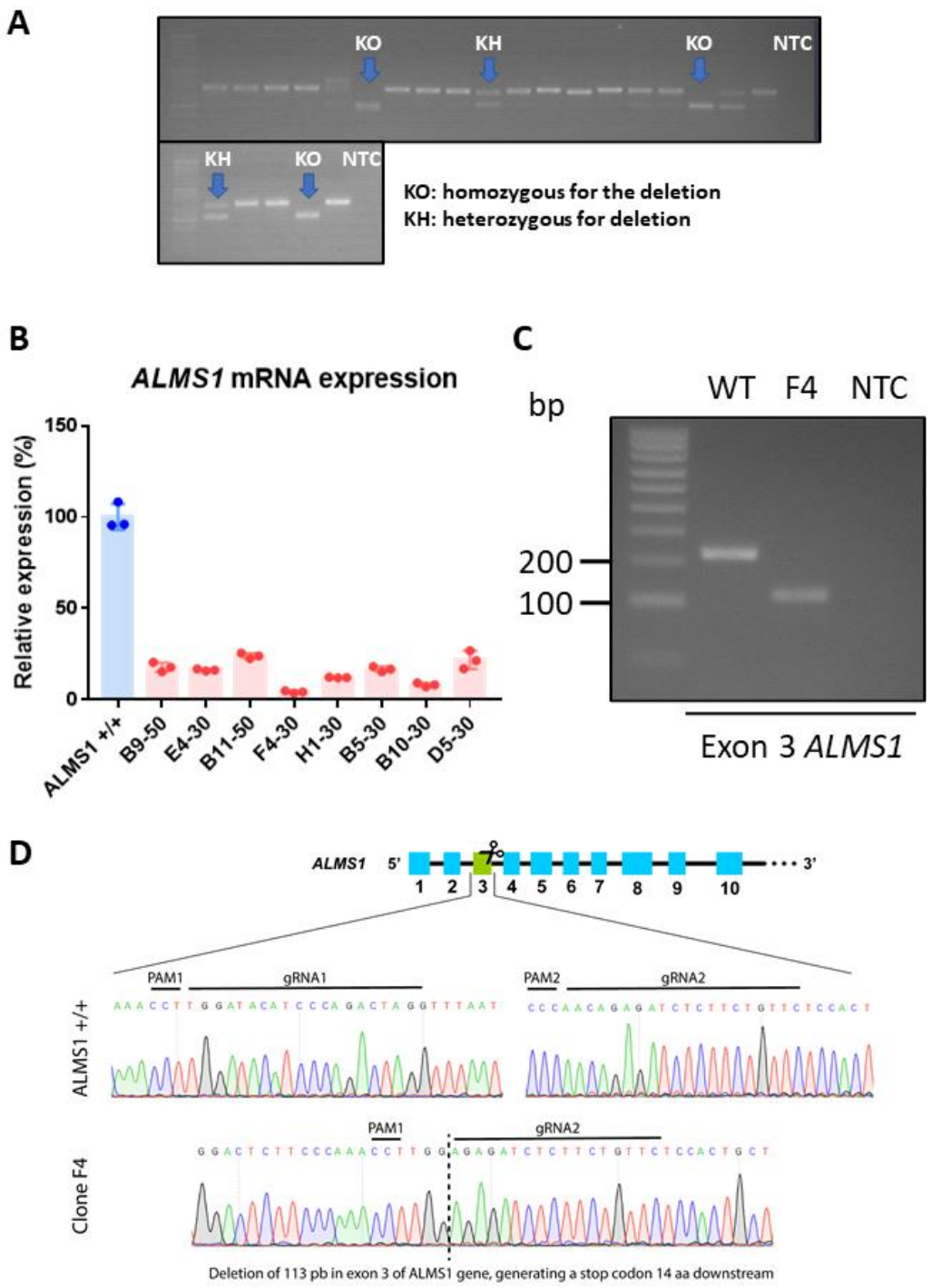

Supplementary Figure S2. Genetic characterisation of *ALMS1* -/- cell line BJ-5ta. **(A)** Clone screening. **(B)** Relative gene expression of ALMS1 +/+ and a batch of clones for ALMS1 -/- genotype. **(C)** Agarose gel (2%) showing the exon 3 amplicon of the control line (ALMS1 +/+) and the F4 clone (ALMS1 -/-) which showed the lowest gene expression. **(D)** Characterisation of the F4 clone mutation by sanger sequencing.